Macromolecules

pubs.acs.org/Macromolecules Article

Rheocoalescence: Relaxation Time through Coalescence of Droplets

Sarath Chandra Varma, Abhineet Singh Rajput, and Aloke Kumar*

Cite This: *Macromolecules* 2022, 55, 6031–6039 Read Online

ACCESS | Metrics & More | Article Recommendations | Supporting Information

ABSTRACT: The dynamics of the pendant drop coalescing with a sessile drop to form a single daughter droplet is known to form a bridge. The bridge evolution begins with a point contact between the two drops leading to a liquid neck of size comparable to the diameter of the drops. To probe this phenomenon in polymeric fluids, we quantify the neck radius growth during coalescence using high-speed imaging. In this study, we unveil the existence of three regimes on the basis of concentration ratio c/c^*, namely, inertioelastic $c/c^* < c_e/c^*$, viscoelastic $c_e/c^* < c/c^* < 20$, and elasticity dominated regimes $c/c^* > 20$. Our results suggest that the neck radius growth with time (t) obeys a power-law behavior t^b, such that the coefficient b has a steady value in inertioelastic and viscoelastic regimes, with a monotonic decrease in elasticity dominated regime. On the basis of this dependence of b on concentration ratios, we propose a new measurement technique, rheocoalescence, which possibly can predict the relaxation time of these fluids in the elasticity dominated regime. We also show a deviation from universality proposed in the literature for the elasticity dominated regime.

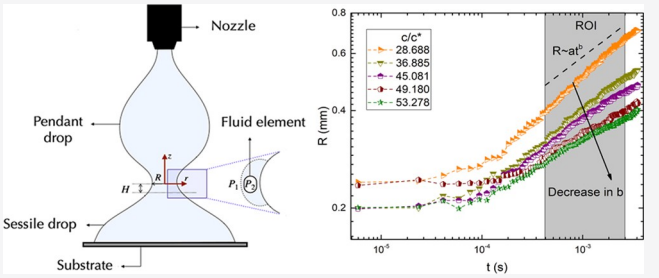

INTRODUCTION

Coalescence is a singular event in which two or more drops merge to form a single daughter droplet.[1] The dynamics of this singular event is governed by the liquid bridge formation and its growth. This temporal growth bears the signature of the underlying governing equation.[2] Such natural processes are observed in raindrop condensation[3,4] and industrial processes such as paint spray coatings,[5,6] combustion process,[7] droplets on surfaces,[8] and processes linked to life.[9,10] Depending on the relative orientation of droplets, the phenomenon can occur in physically different configurations, i.e., pendant−pendant,[11−13] sessile−pendant,[14] and sessile−sessile.[15−17] The entire evolution process in pendant−pendant and sessile−pendant configurations is driven by a balance between surface tension, viscous and inertial effects, and Laplace pressure.[2,13] In Newtonian fluids, based on the force balance, the evolution lies in either the inertia dominated[18] or viscosity dominated regime.[11,12] Apart from these regimes, a new regime of inertially limited viscous regime[19] was proposed in Newtonian droplet coalescence, wherein all inertial, viscous, and surface tension forces are essential.

The kinematics of the coalescence phenomenon in pendant−pendant and sessile−pendant configurations is characterized by the temporal evolution of the liquid bridge of neck radius R and bridge semiwidth H. In Newtonian droplets, the temporal evolution of the neck[12] was demonstrated to follow the scale of $R \sim t^b$, where R is the neck radius and t is time. Based on the viscosity of the fluid, the dynamics of the neck radius evolution has been identified to have a dominant viscous regime at early times and an inertial regime at later instances. In the viscous regime,[12] the neck radius has a scaling of $R \sim t$. Similarly in the inertial regime,[12,18] the neck radius has a scale of $R \sim t^{0.5}$. In the literature, regime-wise universality[2,11−13,18,20−32] is elucidated both experimentally and analytically. In the viscous regime,[18] the neck radius has a universal scaling of $R^* \sim (t^*)$, in which $R_c = R_o$ and $t_c = \eta R_o/\sigma$, where R_o is the radius of the drop, η is the viscosity, and σ is the surface tension. Similarly, in the inertial regime[2,18] the neck radius has a universal scale of $R^* \sim (t^*)^{0.5}$, in which $R_c = R_o$ and $t_c = \sqrt{\rho {R_o}^3/\sigma}$, with ρ being the density.

The paradigm of coalescence phenomenon in rheologically complex fluids is significantly more involved. Polymeric fluids are a distinct subgroup of complex fluids that exhibit strong non-Newtonian characteristics due to molecular chain interactions or relaxations. The relaxation time (λ) is the fingerprint of elasticity and molecular relaxations. Recently, Fardin et al.[33] showed that the coalescence, spreading, and pinching of drops are qualitatively similar on the basis of the Ohnesorge number, *Oh*, relating viscosity, surface tension, and density. However, in polymeric fluids, the fluid relaxation time along with *Oh* distinguishes the coalescence, spreading, and capillary breakup phenomena from Newtonian behavior.

Received: February 2, 2022
Revised: May 11, 2022
Published: May 28, 2022

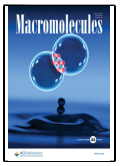

https://doi.org/10.1021/acs.macromol.2c00249
Macromolecules 2022, 55, 6031−6039

Kinematic similarity is retained in all these phenomena, but the dynamic similarity is affected due to the addition of elastic forces. A recent study of aqueous solutions of polymer droplets on both pendant−sessile[14] and sessile−sessile[15] configurations emphasized the role of relaxation time on the dynamics of neck radius evolution. The former study of pendant−sessile[14] configuration showed that for $Wi \sim O(1)$, where $Wi = \lambda U/R$ (λ is relaxation time and U is neck velocity) is the Weissenberg number, the neck radius growth follows the scale of $R \sim t^{0.36}$. The study also showed that for $Wi \sim O(10^{-3}-10^{-4})$ the neck radius growth follows the scale of $R \sim t^{0.39}$. The study also showed a universal scaling of $R^* \sim t^{*0.36}$ in the coalescence of polymeric droplets by nondimensionalizing the neck radius and time with $R_c = \sqrt{\nu_o \lambda}$ and $t_c = Oh\lambda(c/c^*)^{1.2}$, respectively, where ν_o is the kinematic viscosity of the fluid, λ is the relaxation time, Oh is the Ohnesorge number, and c/c^* is the concentration ratio. Recently, a numerical study by Chen et al.[34] showed the effect of polymer chain relaxation on the coalescence process. This study is in qualitative agreement with our previous results[14] showing the deviation from Newtonian droplets' coalescence. Similar to the relaxation time, the concentration ratio c/c^* is another important parameter representing the chain entanglements. Our previous study[14] on coalescence of polymeric droplets was done on the solutions of $c/c^* < 10$. In this study we investigate the coalescence of the polymeric droplets with $c/c^* > 10$.

Despite many applications of coalescence of polymeric droplets in microfluidics and interfacial rheology,[35,36] this phenomenon is sparsely studied. In this study, we demonstrate that the coalescence of sessile and hanging pendant drops of aqueous polymer solutions has different regimes, along with the dependence of neck growth on the relaxation time. To experimentally depict the effect of relaxation time on neck growth, we study the coalescence of droplets for various concentrations of poly(ethylene oxide) (PEO) of molecular weights $M_w = 5 \times 10^6$ and 4×10^6 g/mol. The experimental observation of neck radius growth of various concentrations is demonstrated by scaling analysis based on the linear Phan−Thein−Tanner (PTT)[37,38] constitutive equation. Our results contrast the universal behavior proposed previously and hold enormous promise for opening a new method to determine the relaxation time of the fluid.

MATERIALS AND METHODS

Poly(ethylene oxide) (PEO) of different molecular weights M_w are added to DI water in sufficient quantities to get the various concentrations c. All the solutions are stirred at 300 rpm for different durations. Polymers used in this study along with their molecular weights are listed in Table 1. Concentrations of the polymers are chosen in a way that the solution types vary in a range of semidilute unentangled and semidilute entangled regimes. Regimes of semidilute unentangled and semidilute entangled are differentiated by using the critical concentration c^* and the entanglement concentration c_e, respectively. The critical concentration of PEO for different molecular weights is obtained from the $[\eta]$ intrinsic viscosity by using the Flory relation $c^* = 1/[\eta]$ alongside the Mark−Houwink−Sakurada correlation[39] $[\eta] = 0.072M_w^{0.65}$, and the entanglement concentration c_e is obtained by using the relation $c_e \approx 6c^*$.[40] The values of c^* and c_e are listed in Table 1. All the concentrations used in present study along with their concentration ratios c/c^* are given in Table 2.

Table 1. List of Molecular Weights of Polymers along with Their Critical and Entanglement Concentrations

polymer	M_w (g/mol)	c^* (% w/v)	c_e (% w/v)
PEO	5×10^6	0.061	0.366
PEO	4×10^6	0.071	0.426

Table 2. Rheological Properties of the Solutions[a]

M_w (g/mol)	c (% w/v)	c/c^*	η_o (Pa·s)	n	Γ (s)	λ (s)
5×10^6	0.1	1.64	0.006			0.0017*
	0.2	3.28	0.018	0.757	0.04	0.0025*
	0.4	6.56	0.06	0.427	0.04	0.042*
	0.75	12.29	0.8	0.358	0.34	0.165*
	1	16.39	4.5	0.240	3.18	0.5
	1.5	24.59	20	0.305	2.98	0.67
	1.75	28.68	40	0.285	4.03	1.325
	2.25	36.88	72	0.250	4.27	1.43
	2.5	40.98	85	0.241	3.60	1.59
	2.75	45.08	190	0.218	2.13	2.0
	3	49.18	210	0.240	4.80	2.25
	3.25	53.28	230	0.213	4.86	2.5
4×10^6	0.5	7.04	0.038	0.679	0.03	0.058*
	1.0	14.08	0.6	0.298	4.86	0.25
	1.5	21.13	2	0.264	3.098	0.57
	2.0	28.17	10	0.508	4.74	1.04
	2.5	35.21	16	0.443	5.06	1.65
	3.0	42.25	75	0.453	6.06	2.4

[a]Relaxation time values indicated with an asterisk are obtained from the correlations. The remaining values are obtained from the crossover of G' and G''.

Experiments are performed on a polydimethylsiloxane (PDMS)-coated glass substrate. Before the experiments the substrates are cleaned with detergent followed by sonication with acetone and DI water for 20 min each. The substrates are then dried in a hot air oven 95 °C for 30 min. PDMS is prepared by adding the curing agent (Syl Gard 184 Silicone Elastomer Kit, Dow Corning) to PDMS in the ratio of 1:10. This mixture is agitated and kept for desiccation for 30 min until all visible gas bubbles are removed. Glass substrates are coated with PDMS by using a spin coater at 5000 rpm for 60 s. The coated substrates are cured by keeping them in a hot air oven at 90 °C for at least 90 min. The initial contact between the drops was achieved by bringing the two droplets of constant volume toward each other with a certain approach velocity. The surface tension σ of the solutions is measured by the pendant drop method using an optical contact angle measuring and contour analysis system (OCA25) instrument from Dataphysics. All the solutions were found to have surface tension values of 0.062 ± 0.03 N/m. We have assumed the density of all the solutions to be 1000 kg/m^3.

Rheology. *Rheometry.* Rheology experiments are performed on an Anton Paar MCR 302 rheometer using a cone and plate 40 mm, 1° geometry to characterize the viscoelastic behavior of the solutions. The viscosity variation with shear rate for the chosen solutions is shown in Figure 1a. All the concentrations have shown the shear thinning behavior. The zero shear viscosity of the solutions is obtained by fitting the viscosity data in the form of Carreau−Yasuda model[41] represented by the equation $\eta - \eta_\infty = (\eta_o - \eta_\infty)[1 + (\Gamma\dot{\gamma})^p]^{(n-1)/p}$, where η_o, η_∞, $\dot{\gamma}$, n, Γ, and p represent zero-shear viscosity, infinite-shear viscosity, shear rate, flow behavior index, time constant, and width of the transition region between η_o and the power-law region, respectively. The values of η_o, n, and Γ for all the concentrations are listed in Table 2. The viscoelasticity of the polymer solutions is characterized by performing the small-amplitude oscillatory shear SAOS experiments in the rheometer. The variation of storage modulus G' and loss modulus G'' with frequency ω is shown in Figure 1b for 1, 1.5, 2.25, 2.75, and 3.25% w/v concentrations as a representation.

https://doi.org/10.1021/acs.macromol.2c00249
Macromolecules 2022, 55, 6031−6039

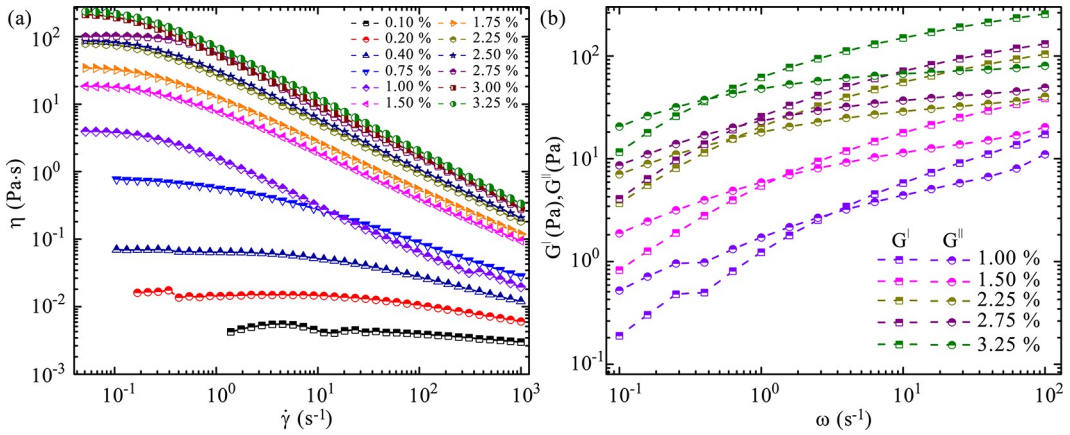

Figure 1. Rheological behavior of PEO ($M_w = 5 \times 10^6$ g/mol). (a) Dependence of viscosity on shear rate for different concentrations. (b) Variation of the storage modulus G' and the loss modulus G'' with frequency obtained from SAOS experiments for 1, 1.5, 2.25, 2.75, and 3.25% w/v concentrations (standard deviation of the data is <2% for all the concentrations).

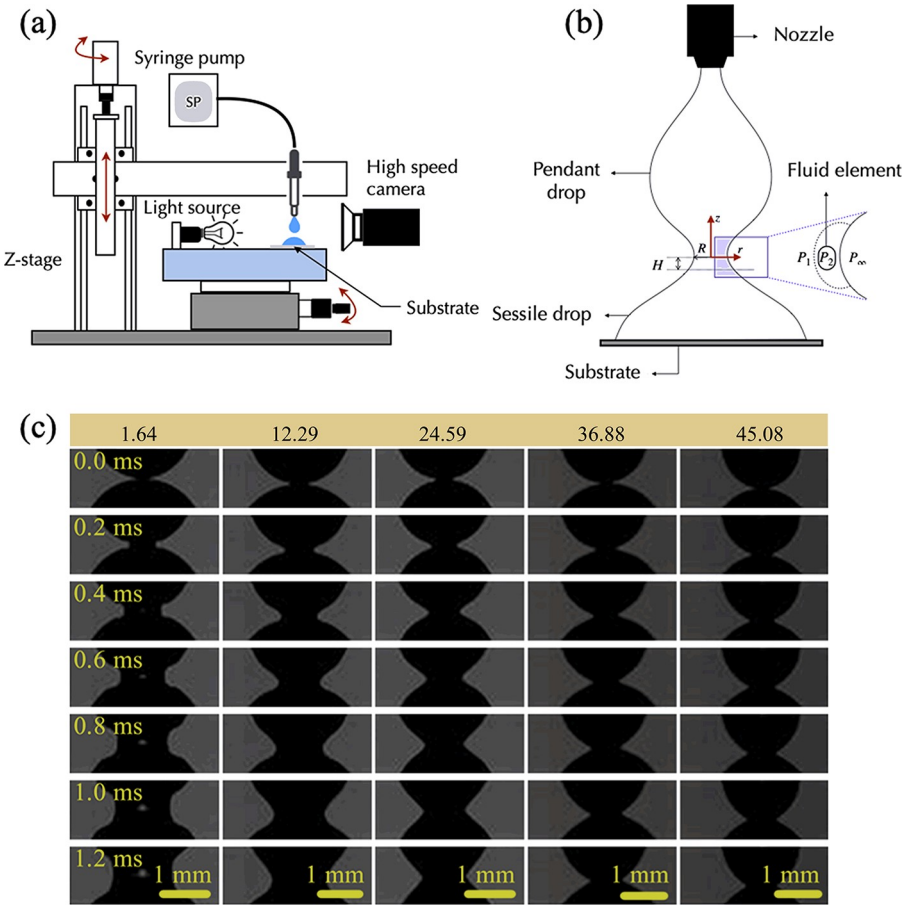

Figure 2. Schematics of (a) the experimental setup, (b) the neck region during coalescence representing the geometrical parameters during the process, and (c) the neck radius evolution of various concentration ratios: 1.64, 12.29, 24.59, 36.88, and 45.08 of PEO at different instants.

Relaxation Time. In SAOS, the relaxation time λ of the polymer solutions is defined as $\lambda = 1/\omega_c$, where ω_c is the crossover frequency for the G' and G'' curves. It is observed that for concentrations $c > 1\%$ w/v SAOS has a crossover. But for $c < 1\%$ w/v, there is no crossover as rheometer has the maximum frequency of 100 s^{-1}, which corresponds to time scale of 10^{-2} s. Therefore, for $c < 1\%$ w/v, the relaxation times are estimated by using the Zimm model.[41]

$$\lambda_z = \frac{1}{\zeta(3\nu)} \frac{[\eta] M_w \eta_s}{N_A k_B T} \tag{1}$$

where η_s is the solvent viscosity, k_B is the Boltzmann constant, λ_z is the Zimm relaxation time, T is the absolute temperature, and ν is fractal polymer dimension determined via the relation $a = 3\nu - 1$, where a is the exponent of the Mark−Houwink−Sakurada correlation. For the solutions in the semidilute unentangled λ_{SUE} and semidilute entangled λ_{SE} regimes, the relaxation times are calculated by using these correlations $\lambda_{SUE} = \lambda_z \left(\frac{c}{c^*}\right)^{(2-3\nu)/(3\nu-1)}$ and $\lambda_{SE} = \lambda_z \left(\frac{c}{c^*}\right)^{(3-3\nu)/(3\nu-1)}$ [42−44], respectively. The relaxation times for the chosen concentrations are listed in Table 2. The relaxation times obtained for $c > 1\%$

https://doi.org/10.1021/acs.macromol.2c00249
Macromolecules 2022, 55, 6031−6039

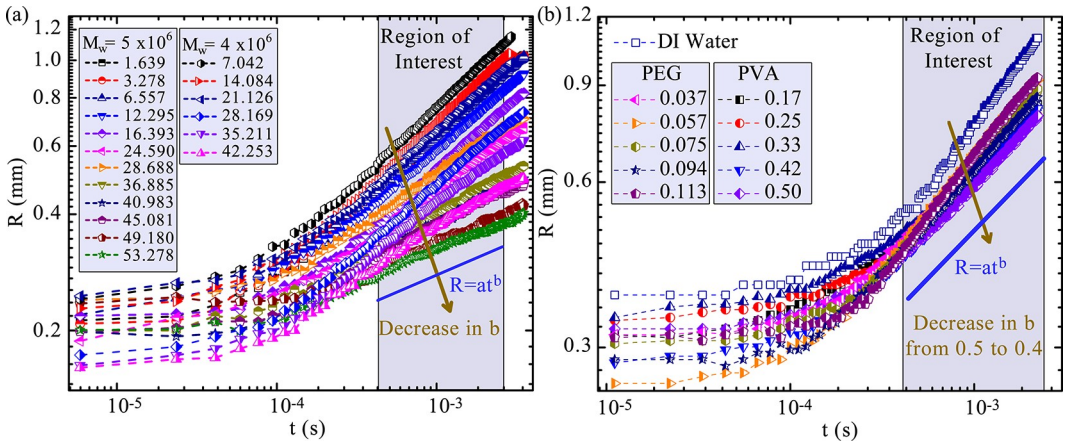

Figure 3. (a) Evolution of neck radius for various concentration ratios $c/c^* > 1$ of PEO solutions showing the decrease in slope b with concentration ratios. (b) Neck radius evolution for $c/c^* < 1$ of poly(ethylene glycol) (PEG) and poly(vinyl alcohol) (PVA), the latter obtained from our previous study Varma et al.,[14] along with DI water ($c/c^* = 0$) representing the decrease in b from 0.5 to 0.4 with addition of polymer (note: the error in the measurements is <5%).

w/v from the crossover frequency of G' and G'' are in good agreement with the Zimm model estimated values. As a representation, the relaxation time obtained from the frequency sweep for 1.5% w/v is 0.67 s compared to the value obtained from the Zimm model as 1 s.

Experiments. A drop of diameter 2.25 ± 0.1 mm is dispensed on a substrate. To achieve coalescence, a pendant drop of the same diameter is brought toward the dispensed drop with 10^{-4} m/s approach velocity to ensure the controlled coalescence. Experiments are conducted at a temperature of 25 °C and a 1 atm pressure. Figure 2a shows the schematic of the experimental setup. The coalescence process is captured at 170000 fps by using a Photron Fastcam mini high-speed camera with a Navitar lens attachment. The drops are illuminated by using an LED light source. Data extraction from the images is performed by using custom-written algorithms in MATLAB.

RESULTS AND DISCUSSION

Coalescence proceeds via the formation of a liquid bridge during the merge of a pendant and sessile drop. This phenomenon is characterized by two geometric parameters, namely, the neck radius R and the neck semiwidth H as shown in Figure 2b. The neck radius grows with time due to the local curvature effects caused by surface tension σ. Such growth of neck radius for the concentration ratios 1.64, 12.29, 24.59, 36.88, and 45.08 of PEO $M_w = 5 \times 10^6$ g/mol at different time instants is shown in Figure 2c. It is evident from Figure 2c that for a particular time instant the bridge curvature for different concentration ratios has a significant change as the ratio increases.

The temporal evolution of the neck radius for various concentration ratios of the polymeric drops is shown in Figure 3. The neck radius growth for the concentration ratios represented in Figure 3a are the averaged values of five trials. It can be seen that the bridge has slow growth initially followed by faster growth. As previously reported in the literature, it is seen that the neck growth follows the universal power-law growth function[14] $R = at^b$, which is equivalently the linear regime in Figure 3. For different concentration ratios of polymeric droplets, there is a decrease in neck speed due to the change in neck curvature. This is reflected in the power law index b. The variation of b for different concentration ratios of polymeric droplets is illustrated in Figure 3a. For $M_w = 5 \times 10^6$ g/mol the value of b ranges from 0.38 to 0.16, while for $M_w = 4 \times 10^6$ g/mol the value of b ranges from 0.39 to 0.25 for the range of concentration ratios explored in this study. The sample analysis for three trials of different concentration ratios in the linear−linear axis is shown in Figure S1. The error in these fitting is less than 5%, with an R^2 of a minimum of 99%. Figure 3b shows the neck radius evolution of poly(ethylene glycol) (PEG) and poly(vinyl alcohol) (PVA) obtained from our previous study Varma et al.[14] for $c/c^* < 1$ along with DI water $c/c^* = 0$, indicating the decrease in slope from 0.5 to 0.4.

To elucidate the coalescence dynamics in polymeric fluid droplets, it is crucial to outline the underlying forces. These underlying forces are capillary force F_c, inertial force F_i, viscous force F_v, and elastic force F_e. Among these forces, F_c drives the bridge growth while the other three forces oppose it. The effect of these opposing forces F_i, F_v, and F_e can be captured by three nondimensional numbers: Reynolds number $Re = \langle \rho u_c l_c/\eta_o \rangle$, $Wi = \langle \lambda u_c/l_c \rangle$, and elasticity number $El = \langle \eta_o \lambda/\rho l_c^2 \rangle$, where u_c and l_c represent characteristic velocity and length scales, respectively, ρ is the density, and η_o is the zero shear viscosity. The characteristic scales associated with the flow are $u_c \sim \partial R/\partial t$ and $l_c \sim R$. The data corresponding to $c/c^* = 4.22$ and 5.63 of $M_w = 4 \times 10^6$ g/mol in the subsequent diagrams are obtained from our previous study Varma et al.[14] The variation of these nondimensional numbers with concentration ratio c/c^* is presented in Figure 4. It reveals the presence of three

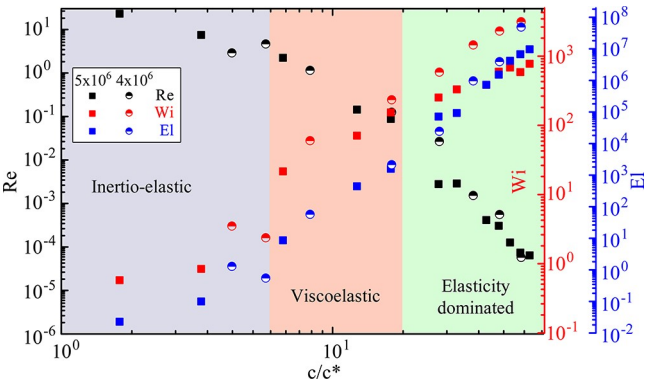

Figure 4. Nondimensional numbers, Reynolds number, Weissenberg number, and Elasticity number calculated from experimental data at different c/c^* for PEO of different molecular weights. Three regimes, viz., inertioelastic, viscoelastic, and elasticity dominated regimes, can be seen.

https://doi.org/10.1021/acs.macromol.2c00249
Macromolecules 2022, 55, 6031−6039

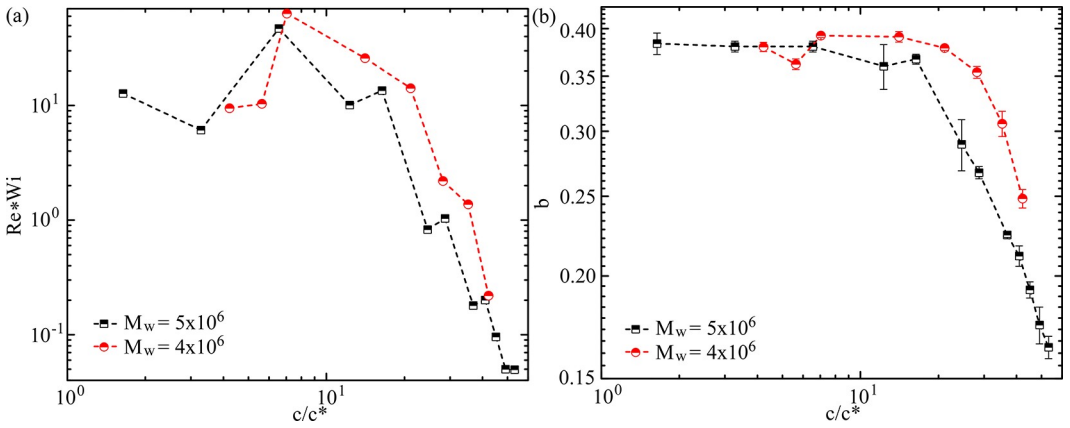

Figure 5. (a) Variation of Re^*Wi with c/c^* representing the decrease in Re^*Wi from $O(10^1)$ to $<O(10^0)$ from the inertioelastic/viscoelastic to the elasticity dominated regime. (b) Steady and monotonic decrease of b in inertioelastic/viscoelastic regimes ($c/c^* < 20$) and the elasticity dominated regime ($c/c^* > 20$), respectively.

regimes based on the concentration ratios. In the first regime with concentration ratios $c/c^* < c_e/c^*$, the orders of corresponding numbers are $Re \sim O(10)$, $Wi \sim O(10^0)$ and $El \sim O(10^{-1})$, suggesting the dominance of inertia force over viscous and elastic forces i.e. $F_i > F_v \approx F_e$. As the inertial forces are predominant, this regime is an inertioelastic coalescence. While for the second regime, with the concentration ratios $c_e/c^* < c/c^* < c_c/c^*$ ($c_c/c^* \approx 20$), $Re \sim O(10^{-1})$, $Wi \sim O(10)$, and $El \sim O(10^2)$, indicating that $F_e > F_v > F_i$. Here c_c/c^* is the concentration ratio at which the regime shifts from the viscoelastic to elasticity dominated regime. As the elastic forces are predominant followed by the viscous forces, this regime is a viscoelastic coalescence. Similarly, for the regime with $c/c^* > c_c/c^*$, $Re < O(10^{-1})$, $Wi > O(10^2)$, and $El > O(10^3)$, indicating that $F_e \gg F_v \gg F_i$. In this regime, the elastic forces are much greater than viscous forces, making it an elasticity dominant coalescence. As we increase the value of c/c^*, the coalescence phenomenon shifts from inertioelastic to elasticity dominated regime. It is observed from Figure 3a that the solutions in inertioelastic and viscoelastic regimes have a constant slope of 0.37, whereas, in the elastic dominated regime, there is a continuous decrease in slope with c/c^*. In Newtonian fluids, $F_e = 0$ suggests that the phenomenon has two regimes: viscous and inertial. For polymeric fluids, as discussed above, the capillary force is balanced by the combination of inertial and elastic forces in the inertioelastic regime, which reduces b from 0.5 to 0.37. The value of 0.36 ± 0.02 in the inertioelastic regime is demonstrated in our previous studies[14] both experimentally and semianalytically. Similarly, in the viscoelastic regime, the capillary force is balanced by the combination of elastic and viscous forces, resulting in a b value of 0.37. The decrease in slope from 1 (viscous regime[32]) to 0.37 (viscoelastic regime) is more pronounced than the decrease in slope from 0.5 (inertial regime[32]) to 0.37 (inertioelastic regime) as $O(F_e + F_v) > O(F_e + F_i)$. However, $O(F_e + F_v)$ and $O(F_e + F_i)$ exhibit a weak dependence on c/c^* in their respective regimes, resulting in a constant slope of 0.37. On the contrary, the capillary force is balanced by elastic force in the elasticity dominated regime. As $O(F_e)$ has a strong dependence on c/c^*, a continuous decrease in b with c/c^* can be observed in this region.

The effect of the predominant forces in above three regimes are expounded by nondimensionalizing the radial r direction momentum equation under the quasi-radial assumption. The flow inside the coalescing drops is quasi-radial and quasi-steady with a localized vortex in the small region near the neck for Newtonian fluids. The detailed study of flow inside the coalescing droplets is shown by Xia et al.[32] For polymeric droplet coalescence, the flow field is similar to Newtonian coalescence in the inertioelastic and viscoelastic regimes. However, in the elasticity dominated regime, the flow is no longer quasi-steady as the temporal variation of the stresses cannot be neglected. The gravitation force is neglected in the momentum equation as the Bond number $Bo = \rho g R_o^2/\sigma$ is of $O(10^{-1})$ in this study. The nondimensional variables are defined as $v_r^* = v_r/u_c$, $r^* = r/R$, $z^* = z/R$, $t^* = t/T$, $\tau_{rr}^* = \tau_{rr}/\tau_{RC}$, $\tau_{rz}^* = \tau_{rz}/\tau_{ZC}$, and $p^* = p/P_c$, where $T := R/u_c$ and $P_c := \sigma/R_o$ (R_o is the droplet radius) are the characteristic time and pressure, respectively. Thus, the r-direction momentum equation takes the form

$$\frac{\rho u_c^2}{R}\left(\frac{\partial v_r^*}{\partial t^*} + v_r^*\frac{\partial v_r^*}{\partial r^*}\right) = -\frac{P_c}{R}\frac{\partial p^*}{\partial r^*} + \frac{\tau_{RC}}{R}\left(\frac{\tau_{rr}^*}{r^*} + \frac{\partial \tau_{rr}^*}{\partial r^*}\right) + \frac{\tau_{ZC}}{R}\frac{\partial \tau_{rz}^*}{\partial z^*} \tag{2}$$

The characteristic scales of stresses τ_{RC} and τ_{ZC} are obtained by introducing the previously defined nondimensional variables, along with the quasi-radial assumption in the linear Phan–Thein–Tanner constitutive equation as follows:

$$\frac{\partial \tau_{rr}^*}{\partial t^*} + v_r^*\frac{\partial \tau_{rr}^*}{\partial r^*} - 2\tau_{rr}^*\frac{\partial v_r^*}{\partial r^*} + \frac{\tau_{rr}^*}{\frac{\lambda U}{R}}\left[1 + \frac{\kappa\lambda}{\eta}\tau_{RC}\tau_{rr}^*\right] = 2\frac{\eta}{\lambda\tau_{RC}}\frac{\partial v_r^*}{\partial r^*} \tag{3}$$

$$\frac{\partial \tau_{rz}^*}{\partial t^*} + v_r^*\frac{\partial \tau_{rz}^*}{\partial r^*} - \tau_{rz}^*\frac{\partial v_r^*}{\partial r^*} + \frac{\tau_{rz}^*}{\frac{\lambda U}{R}}\left[1 + \frac{\kappa\lambda}{\eta}\tau_{RC}\tau_{rr}^*\right] = \frac{\eta}{\lambda\tau_{ZC}}\frac{\partial v_r^*}{\partial z^*} \tag{4}$$

From eqs 3 and 4 it is observed that $\tau_{RC} := \eta/\lambda$ and $\tau_{ZC} := \eta/\lambda$. By substitution of these scales into eq 2, the dimensionless radial momentum equation is deduced as represented in eq 5.

$$\frac{\rho u_c^2\lambda}{\eta}\left(\frac{\partial v_r^*}{\partial t^*} + v_r^*\frac{\partial v_r^*}{\partial r^*}\right) = -\frac{\sigma\lambda}{\eta R_o}\frac{\partial p^*}{\partial r^*} + \frac{\tau_{rr}^*}{r^*} + \frac{\partial \tau_{rr}^*}{\partial r^*} + \frac{\partial \tau_{rz}^*}{\partial z^*} \tag{5}$$

https://doi.org/10.1021/acs.macromol.2c00249
Macromolecules 2022, 55, 6031−6039

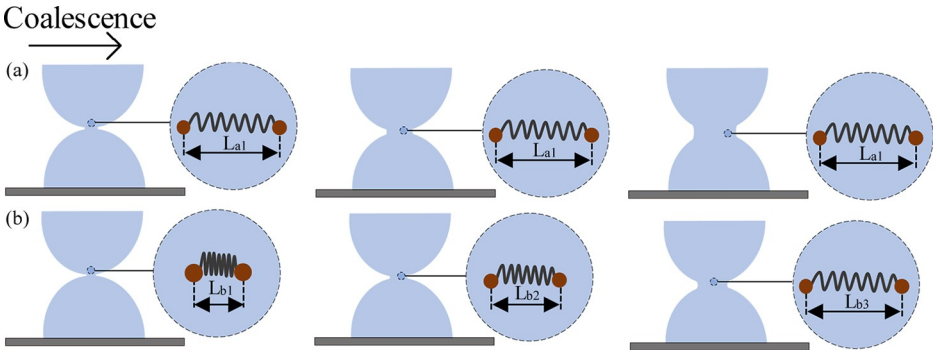

Figure 6. Schematic of the chain behavior at different time instances during coalescence (left to right) of solutions in (a) inertioelastic and viscoelastic regimes showing the constant conformation length L_{a1} and (b) elasticity dominated regime showing the conformation lengths as $L_{b3} > L_{b2} > L_{b1}$.

The coefficient $\frac{\rho u_c^2 \lambda}{\eta}$ of the inertial term in eq 5 is the product of Re and Wi, which is given as $Re^*Wi = \langle \rho u_c^2 \lambda/\eta \rangle = \frac{\text{elastic force} \times \text{inertia force}}{(\text{viscous force})^2}$. The term Re^*Wi can be rewritten as $Re^*Wi = \langle u_c^2/U_s^2 \rangle$, where $U_s = \sqrt{\eta/\rho\lambda}$[45] is the shear wave velocity of the complex fluid. The values of Re^*Wi are presented for different concentration ratios in the Figure 5a. In the elasticity dominated regime, as observed in Figure 4, the product of Re and Wi is $Re^*Wi = \langle u_c^2/U_s^2 \rangle < O(10^0)$, while for the other regimes $Re^*Wi \sim O(10^1)$. This implies that for the elasticity dominated regime the characteristic velocity of the system u_c is less than the shear wave velocity of the fluid U_s while $u_c > U_s$ for the other regimes. The polymer chains begin to elongate along the shear direction after the droplets have touched each other. Such elongation decreases as the concentration of polymer increases due to polymer chain entanglements which alter the curvature of the liquid bridge, leading to the slow growth of the bridge and inhibiting the coalescence. In the elasticity dominated regime, the chains relax slower than the speed of information transfer; hence, the polymer chains are in the unrelaxed state. On the contrary, for the other regimes, the polymer chains relax faster than the speed of information transfer, implying that the chains have already relaxed to the external perturbation. This behavior can be interpreted with a simple analogy by considering the simple shear flow of high and low Weissenberg numbers as studied by Huang et al.[46] Their study showed that at small Weissenberg numbers the polymers are only weakly perturbed and are close to their equilibrium conformations, whereas large Wi implies large deformations and a strong alignment with flow. As observed from Figure 6a, in inertioelastic and viscoelastic regimes, the conformation of the chain is elongated to length L_{a1} when the drops touch each other. They remain in that conformation throughout the process and move along with the neck, whereas in the elasticity dominated regime the conformation is in an unrelaxed state. This conformation of the chains continuously changes as the process proceeds, as represented in Figure 6b, where $L_{b1} < L_{b2} < L_{b3}$. The rate of change in conformation is dependent on the elasticity of the fluid. This temporal change in conformations leads to increase in elasticity, thereby inhibiting the neck growth and reducing power law index b in elasticity dominated regime where $Re^*Wi < O(10^0)$ as represented in Figure 5b.

The effect of chain relaxation time is further demonstrated by considering the characteristic velocity u_c as the chain relaxation velocity, which can be defined as $u_c = R_o/\lambda$. On substitution, the term $\rho u_c^2 \lambda/\eta$ can be simplified as $\rho R_o^2/\eta\lambda$. This simplified result can be rewritten as the ratio of time scales (τ^*) $\rho R_o^2/\eta\lambda = t_c/\lambda = 1/\tau^{*2}$ where $t_c = t_i^2/t_v$ is the Newtonian characteristic time. Here, $t_v = \eta R_o/\sigma$ is the viscous time scale and $t_i = \sqrt{\rho R_o^3/\sigma}$ is the inertial time scale. It is observed from Figure 7 that when $\tau^* < 10$, the exponent is

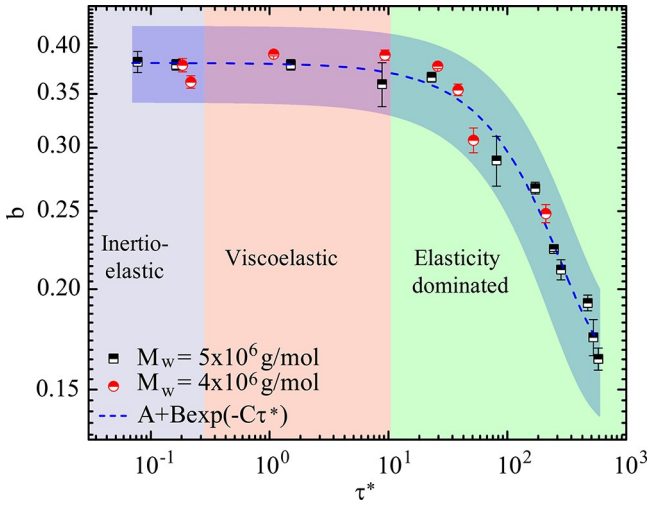

Figure 7. Dependence of the power law index b on τ^* (ratio of relaxation time λ and Newtonian characteristic time t_c). The dashed blue line represents the exponential fit of 97% confidence interval with $A = 0.15871 \pm 0.01452$, $B = 0.22368 \pm 0.01409$, and $C = 0.0048 \pm 0.00068$ for PEO solutions of different molecular weights and the shades represents the error bounds of the fit.

constant with a value of 0.37; i.e., the process is in an inertioelastic or a viscoelastic regime. On the contrary, when $\tau^* > 10$, the exponent decreases continuously. The dynamics governing the above phenomenon lies in the relaxing of polymer chains. When $\tau^* < 10$, the polymer chain relaxation are comparable to the Newtonian time scale t_c, leading to a constant value. However, for $\tau^* > 10$, the polymer chains are in unrelaxed state even after the Newtonian time scale therefore altering the curvature of the bridge, resulting in the decline of b.

The universal behavior of the neck radius evolution is proposed in our previous study Varma et al.[14] in the

https://doi.org/10.1021/acs.macromol.2c00249
Macromolecules 2022, 55, 6031−6039

inertioelatic regime. To attain the universality, we nondimensionalized the neck radius R by using $\sqrt{\nu_o\lambda}$ as $R^* = R/\sqrt{\nu_o\lambda}$. Similarly, time t is nondimensionalized with $\lambda Oh^{-1}\left(\frac{c}{c^*}\right)^{-1.2}$ leading to $t^* = \left(\frac{t}{\lambda}Oh^{-1}\right)\left(\frac{c}{c^*}\right)^{-1.2}$. This nondimensionalization led to the universal behavior of the neck radius growth as $R^* \sim t^{*0.36}$, which is in agreement with the solutions in the inertioelastic and viscoelastic regimes having a constant value of $b = 0.37$ as represented in Figure 8. However,

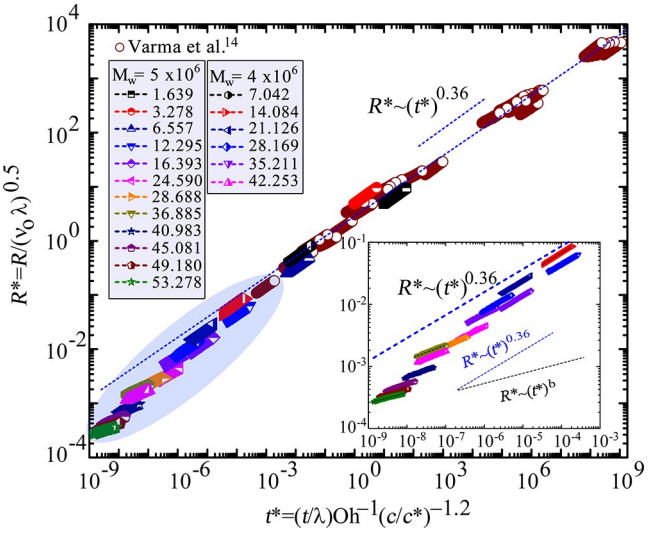

Figure 8. Nondimensional neck radius as a function of nondimensional time for all the polymer solutions used in this study and our previous study,[14] with the legend representing corresponding c/c^* values. Inset shows departure from universality for $c/c^* > 10$ highlighted in the shaded region.

such nondimensionalization of neck growth breaks in the elasticity dominated regime. As the low Wi assumption is no longer valid, the previously reported governing equations is unable to capture the deviation from universality. This deviation shown in the inset of Figure 8 is due to the incorrect characteristic length and time obtained from the balance of inertia, elastic, and capillary forces, as the inertial forces are weak in the elasticity dominated regime. Moreover, in this regime, the polymer chains are not relaxed; hence, the temporal variation of stress in the upper convected derivative has to be considered, which was neglected in our previous study.[14]

This deviation from universality in the elasticity dominated regime provides a novel method to determine the relaxation time λ of the complex fluids by using the coalescence experiment. From Figure 7 we propose a correlation between τ^* and b as $b = A + B\exp(-C\tau^*)$ with $A = 0.15871 \pm 0.01452$, $B = 0.22368 \pm 0.01409$, and $C = 0.0048 \pm 0.00068$ for PEO. This correlation for PEO is validated by conducting coalescence experiments for concentration ratio $c/c^* = 32.56$ (2.0% w/v) of PEO $M_w = 5 \times 10^6$ g/mol solution having $\eta = 55$ Pa·s. Under similar experimental conditions, the temporal evolution of the neck for $c/c^* = 32.56$ is found to have the power-law exponent as $b = 0.275$. On substituting $b = 0.275$ in the correlation, we obtain the relaxation time as $\lambda = 0.6$ s, which agrees with the relaxation time obtained from the SAOS experiments, 1.35 s. For all chosen concentration ratios with $c/c^* > 10$, the relaxation times obtained from the proposed correlation and the values obtained from the crossover of storage and loss modulus from the rheometer for $M_w = 5 \times 10^6$ and 4×10^6 g/mol are represented in Figures 9a and 9b, respectively. It is observed that the values obtained from the proposed correlation are in good agreement with the rheometer values, whereas for $c/c^* < 10$, fitting is highly sensitive to the fitting constants, leading to large deviations from the measured and theoretical values as shown in Figure S2. This indicates that this method is capable of measuring relaxation times primarily in the elasticity dominated regimes. Even though there are slight differences in the relaxation times, it is known that measured values of relaxation time are method specific. For instance, the relaxation times obtained from the capillary breakup extensional rheometer (CABER)[39,47−49] and SAOS differ by an order. It is also observed that the relaxation times obtained from the proposed correlation in semidilute unentangled and semidilute entangled regimes lie in between the values obtained from Dinic et al.[50] and the Zimm correlation, as the process is not purely extensional.

In the literature, many methods are proposed to measure the relaxation time of a fluid. The most widely used way to find λ is the linear viscoelastic response in a conventional rheometer.[41,51] In this method, material is subjected to sinusoidal deformation to evaluate the viscous and elastic responses via loss modulus G'' and storage modulus G', respectively. The

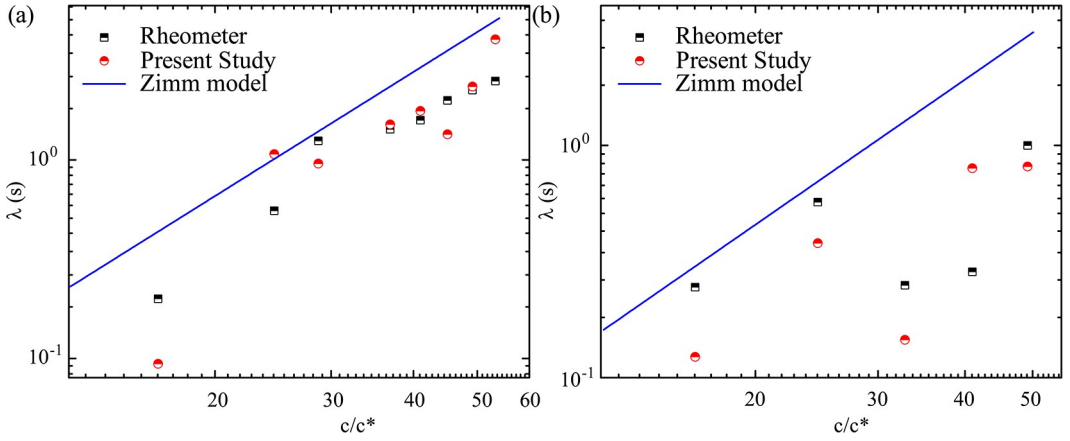

Figure 9. Comparison of relaxation times obtained from the crossover of storage and loss modulus by a rheometer, Zimm model correlations, and this study for $c/c^* > 10$ for (a) $M_w = 5 \times 10^6$ g/mol and (b) $M_w = 4 \times 10^6$ g/mol.

https://doi.org/10.1021/acs.macromol.2c00249
Macromolecules 2022, 55, 6031−6039

crossover of G' and G'' is used to determine the relaxation time of the fluid, but this method is limited by the motor inertia in conventional rheometers and cannot capture the small values of λ. Hence, for low relaxation times, novel methods named CABER, capillary breakup extensional rheometer−dripping on substrate (CABER-DOS),[52−54] and Rayleigh Ohensorge jetting extensional rheometry (ROJER)[55,56] were proposed. However, the intrinsic difficulties in these methods lies in the controlling of elongational flow. Such difficulties have led to significant difference in relaxation times measured from the conventional method and by CABER. Recently, there are developments in microfluidic devices[44,57,58] for overcoming the limitations of conventional rheometer and CABER, but the fabrication of the microfluidic channel is intricate. However, this study proposes a simple comprehensive tool named rheocoalescence based on empirical correlations to determine the relaxation time of PEO solutions. Even though the proposed correlation can be used in all the regimes, it is robust in the elasticity dominated regime. The required experimental information for the correlation can be obtained easily, which makes this tool predominantly effective for cases where performing experiments by conventional methods becomes very difficult such as the case of a highly elastic fluid. This technique potentially opens up a new paradigm in microfluidics and rheological measurements. A comprehensive study of this method is required to generalize rheocoalescence for all the polymeric fluids.

CONCLUSION

The current study demonstrates the effect of fluid elasticity on coalescence of pendant−sessile polymeric droplets. We performed high-speed imaging to capture the temporal evolution of the bridge for a wide range of concentrations ratios. We reveal the presence of three regimes, namely, inertioelastic, viscoelastic, and elasticity dominated regimes, based on c/c^*. The inertioelastic regime occurs at $c/c^* < c_e/c^*$ and and viscoelastic regime at $c_e/c^* < c/c^* < c_c/c^*$; similarly, the elasticity dominated regime occurs at $c/c^* > c_c/c^*$. Experimentally, we have been able to demonstrate the dependence of power-law index b on relaxation time for PEO. This dependence can become the foundation of a novel method, namely rheocoalescence, that has the potential to determine the relaxation time of fluids in the elasticity dominated regime in the absence of experimental rheology data. This potentially opens a new paradigm in determining the characteristic time scales for wider class of complex fluids. However, this study neglects the effect of surrounding fluid on the dynamics by considering air as the outer fluid. Further studies should be dedicated to extend this method's applicability for a variety of fluids along with the effect of an outer fluid.

ASSOCIATED CONTENT

Supporting Information

The Supporting Information is available free of charge at https://pubs.acs.org/doi/10.1021/acs.macromol.2c00249.

Error in power law index b over various experimental trails for different concentrations; comparison of relaxation times obtained from present study and methods proposed in the literature for solutions in semidilute unentangled and semidilute entangled regimes (PDF)

Movie S1: video obtained at 170000 frames/s for c/c^* = 6.56 (AVI)

Movie S2: video obtained at 170000 frames/s for c/c^* = 16.39 (AVI)

Movie S3: video obtained at 170000 frames/s for c/c^* = 36.88 (AVI)

AUTHOR INFORMATION

Corresponding Author

Aloke Kumar − *Department of Mechanical Engineering, Indian Institute of Science, Bangalore 560012, India*; Email: alokekumar@iisc.ac.in

Authors

Sarath Chandra Varma − *Department of Mechanical Engineering, Indian Institute of Science, Bangalore 560012, India*

Abhineet Singh Rajput − *Department of Mechanical Engineering, Indian Institute of Science, Bangalore 560012, India*

Complete contact information is available at: https://pubs.acs.org/10.1021/acs.macromol.2c00249

Notes

The authors declare no competing financial interest.

A version of this manuscript is available at arXiv (10.48550/arXiv.2201.12555.

ACKNOWLEDGMENTS

A.K. acknowledges partial support from DST-SERB, A.S.R. acknowledges partial support from PMRF, and S.C.V. acknowledges the partial support from MHRD.

REFERENCES

(1) Frenkel, J. Viscous flow of crystalline bodies under the action of surface tension. *J. Phys.* **1945**, *9*, 385.

(2) Eggers, J.; Lister, J. R.; Stone, H. A. Coalescence of liquid drops. *J. Fluid Mech.* **1999**, *401*, 293−310.

(3) Villermaux, E.; Bossa, B. Single-drop fragmentation determines size distribution of raindrops. *Nat. Phys.* **2009**, *5*, 697.

(4) Pruppacher, H. R.; Klett, J. D. *Microphysics of Clouds and Precipitation*; Springer: 2010; pp 10−73.

(5) Ashgriz, N.; Poo, J. Coalescence and separation in binary collisions of liquid drops. *J. Fluid Mech.* **1990**, *221*, 183−204.

(6) Djohari, H.; Martínez-Herrera, J. I.; Derby, J. J. Transport mechanisms and densification during sintering: I. Viscous flow versus vacancy diffusion. *Chem. Eng. Sci.* **2009**, *64*, 3799−3809.

(7) Orme, M. Experiments on droplet collisions, bounce, coalescence and disruption. *Prog. Energy Combust. Sci.* **1997**, *23*, 65−79.

(8) Rykaczewski, K.; Scott, J. H. J.; Rajauria, S.; Chinn, J.; Chinn, A. M.; Jones, W. Three dimensional aspects of droplet coalescence during dropwise condensation on superhydrophobic surfaces. *Soft Matter* **2011**, *7*, 8749−8752.

(9) Barbosa, A. D.; Savage, D. B.; Siniossoglou, S. Lipid droplet−organelle interactions: emerging roles in lipid metabolism. *Curr. Opin. Cell Biol.* **2015**, *35*, 91−97.

(10) Wilfling, F.; Haas, J. T.; Walther, T. C.; Farese, R. V., Jr. Lipid droplet biogenesis. *Curr. Opin. Cell Biol.* **2014**, *29*, 39−45.

(11) Paulsen, J. D.; Burton, J. C.; Nagel, S. R. Viscous to inertial crossover in liquid drop coalescence. *Phys. Rev. Lett.* **2011**, *106*, 114501.

(12) Aarts, D. G.; Lekkerkerker, H. N.; Guo, H.; Wegdam, G. H.; Bonn, D. Hydrodynamics of droplet coalescence. *Phys. Rev. Lett.* **2005**, *95*, 164503.

(13) Wu, M.; Cubaud, T.; Ho, C.-M. Scaling law in liquid drop coalescence driven by surface tension. *Phys. Fluids* **2004**, *16*, L51−L54.
(14) Varma, S. C.; Saha, A.; Mukherjee, S.; Bandopadhyay, A.; Kumar, A.; Chakraborty, S. Universality in coalescence of polymeric fluids. *Soft Matter* **2020**, *16*, 10921−10927.
(15) Varma, S. C.; Saha, A.; Kumar, A. Coalescence of polymeric sessile drops on a partially wettable substrate. *Phys. Fluids* **2021**, *33*, 123101.
(16) Ristenpart, W. D.; McCalla, P. M.; Roy, R. V.; Stone, H. A. Coalescence of Spreading Droplets on a Wettable Substrate. *Phys. Rev. Lett.* **2006**, *97*, 064501.
(17) Lee, M. W.; Kang, D. K.; Yoon, S. S.; Yarin, A. L. Coalescence of two drops on partially wettable substrates. *Langmuir* **2012**, *28*, 3791−3798.
(18) Case, S. C.; Nagel, S. R. Coalescence in low-viscosity liquids. *Phys. Rev. Lett.* **2008**, *100*, 084503.
(19) Paulsen, J. D.; Burton, J. C.; Nagel, S. R.; Appathurai, S.; Harris, M. T.; Basaran, O. A. The inexorable resistance of inertia determines the initial regime of drop coalescence. *Proc. Natl. Acad. Sci. U. S. A.* **2012**, *109*, 6857−6861.
(20) Blanchette, F.; Bigioni, T. P. Partial coalescence of drops at liquid interfaces. *Nat. Phys.* **2006**, *2*, 254.
(21) Duchemin, L.; Eggers, J.; Josserand, C. Inviscid coalescence of drops. *J. Fluid Mech.* **2003**, *487*, 167−178.
(22) Hopper, R. W. Coalescence of two equal cylinders: exact results for creeping viscous plane flow driven by capillarity. *J. Am. Ceram. Soc.* **1984**, *67*, C-262−C-264.
(23) Hopper, R. W. Plane Stokes flow driven by capillarity on a free surface. *J. Fluid Mech.* **1990**, *213*, 349−375.
(24) Paulsen, J. D. Approach and coalescence of liquid drops in air. *Phys. Rev. E* **2013**, *88*, 063010.
(25) Paulsen, J. D.; Carmigniani, R.; Kannan, A.; Burton, J. C.; Nagel, S. R. Coalescence of bubbles and drops in an outer fluid. *Nat. Commun.* **2014**, *5*, 3182.
(26) Ristenpart, W.; McCalla, P.; Roy, R.; Stone, H. A. Coalescence of spreading droplets on a wettable substrate. *Phys. Rev. Lett.* **2006**, *97*, 064501.
(27) Yao, W.; Maris, H.; Pennington, P.; Seidel, G. Coalescence of viscous liquid drops. *Phys. Rev. E* **2005**, *71*, 016309.
(28) Decent, S.; Sharpe, G.; Shaw, A.; Suckling, P. The formation of a liquid bridge during the coalescence of drops. *International Journal of Multiphase Flow* **2006**, *32*, 717−738.
(29) Gross, M.; Steinbach, I.; Raabe, D.; Varnik, F. Viscous coalescence of droplets: A lattice Boltzmann study. *Phys. Fluids* **2013**, *25*, 052101.
(30) Sprittles, J.; Shikhmurzaev, Y. Coalescence of liquid drops: Different models versus experiment. *Phys. Fluids* **2012**, *24*, 122105.
(31) Thoroddsen, S. T.; Takehara, K. The coalescence cascade of a drop. *Phys. Fluids* **2000**, *12*, 1265−1267.
(32) Xia, X.; He, C.; Zhang, P. Universality in the viscous-to-inertial coalescence of liquid droplets. *Proc. Natl. Acad. Sci. U. S. A.* **2019**, *116*, 23467−23472.
(33) Fardin, M. A.; Hautefeuille, M.; Sharma, V. Spreading, pinching, and coalescence: the Ohnesorge units. *Soft Matter* **2022**, *18*, 3291−3303.
(34) Chen, S.; Pirhadi, E.; Yong, X. Viscoelastic necking dynamics between attractive microgels. *J. Colloid Interface Sci.* **2022**, *618*, 283−289.
(35) Krebs, T.; Schroën, K.; Boom, R. Coalescence dynamics of surfactant-stabilized emulsions studied with microfluidics. *Soft Matter* **2012**, *8*, 10650−10657.
(36) Vandebril, S.; Vermant, J.; Moldenaers, P. Efficiently suppressing coalescence in polymer blends using nanoparticles: role of interfacial rheology. *Soft Matter* **2010**, *6*, 3353−3362.
(37) Thien, N. P.; Tanner, R. I. A new constitutive equation derived from network theory. *J. Non-Newtonian Fluid Mech.* **1977**, *2*, 353−365.
(38) Phan-Thien, N. A nonlinear network viscoelastic model. *J. Rheol.* **1978**, *22*, 259−283.
(39) Tirtaatmadja, V.; McKinley, G. H.; Cooper-White, J. J. Drop formation and breakup of low viscosity elastic fluids: Effects of molecular weight and concentration. *Phys. Fluids* **2006**, *18*, 043101.
(40) Arnolds, O.; Buggisch, H.; Sachsenheimer, D.; Willenbacher, N. Capillary breakup extensional rheometry (CaBER) on semi-dilute and concentrated polyethyleneoxide (PEO) solutions. *Rheol. Acta* **2010**, *49*, 1207−1217.
(41) Bird, R. B.; Armstrong, R. C.; Hassager, O. *Dynamics of Polymeric Liquids*, 2nd ed.; Wiley: 1987; Vol. *1*.
(42) Rubinstein, M.; Colby, R. H.; et al. *Polymer Physics*; Oxford University Press: New York, 2003; Vol. *23*.
(43) Liu, Y.; Jun, Y.; Steinberg, V. Concentration dependence of the longest relaxation times of dilute and semi-dilute polymer solutions. *J. Rheol.* **2009**, *53*, 1069−1085.
(44) Del Giudice, F.; D'Avino, G.; Greco, F.; De Santo, I.; Netti, P. A.; Maffettone, P. L. Rheometry-on-a-chip: measuring the relaxation time of a viscoelastic liquid through particle migration in microchannel flows. *Lab Chip* **2015**, *15*, 783−792.
(45) Joshi, P.; Shankar, V. Flow-induced resonant shear-wave instability between a viscoelastic fluid and an elastic solid. *Phys. Fluids* **2019**, *31*, 084107.
(46) Huang, C.-C.; Winkler, R. G.; Sutmann, G.; Gompper, G. Semidilute polymer solutions at equilibrium and under shear flow. *Macromolecules* **2010**, *43*, 10107−10116.
(47) Zell, A.; Gier, S.; Rafai, S.; Wagner, C. Is there a relation between the relaxation time measured in CaBER experiments and the first normal stress coefficient? *J. Non-Newtonian Fluid Mech.* **2010**, *165*, 1265−1274.
(48) Meissner, J.; Hostettler, J. A new elongational rheometer for polymer melts and other highly viscoelastic liquids. *Rheol. Acta* **1994**, *33*, 1−21.
(49) Pathak, J. A.; Hudson, S. D. Rheo-optics of equilibrium polymer solutions: Wormlike micelles in elongational flow in a microfluidic cross-slot. *Macromolecules* **2006**, *39*, 8782−8792.
(50) Dinic, J.; Biagioli, M.; Sharma, V. Pinch-off dynamics and extensional relaxation times of intrinsically semi-dilute polymer solutions characterized by dripping-onto-substrate rheometry. *J. Polym. Sci., Part B: Polym. Phys.* **2017**, *55*, 1692−1704.
(51) Larson, R. G. *The Structure and Rheology of Complex Fluids*; Oxford University Press: New York, 1999; Vol. *150*.
(52) Jimenez, L. N.; Dinic, J.; Parsi, N.; Sharma, V. Extensional relaxation time, pinch-off dynamics, and printability of semidilute polyelectrolyte solutions. *Macromolecules* **2018**, *51*, 5191−5208.
(53) Dinic, J.; Zhang, Y.; Jimenez, L. N.; Sharma, V. Extensional relaxation times of dilute, aqueous polymer solutions. *ACS Macro Lett.* **2015**, *4*, 804−808.
(54) Dinic, J.; Sharma, V. Flexibility, extensibility, and ratio of Kuhn length to packing length govern the pinching dynamics, coil-stretch transition, and rheology of polymer solutions. *Macromolecules* **2020**, *53*, 4821−4835.
(55) Keshavarz, B.; Sharma, V.; Houze, E. C.; Koerner, M. R.; Moore, J. R.; Cotts, P. M.; Threlfall-Holmes, P.; McKinley, G. H. Studying the effects of elongational properties on atomization of weakly viscoelastic solutions using Rayleigh Ohnesorge Jetting Extensional Rheometry (ROJER). *J. Non-Newtonian Fluid Mech.* **2015**, *222*, 171−189.
(56) Sharma, V.; Haward, S. J.; Serdy, J.; Keshavarz, B.; Soderlund, A.; Threlfall-Holmes, P.; McKinley, G. H. The rheology of aqueous solutions of ethyl hydroxy-ethyl cellulose (EHEC) and its hydrophobically modified analogue (hmEHEC): Extensional flow response in capillary break-up, jetting (ROJER) and in a cross-slot extensional rheometer. *Soft Matter* **2015**, *11*, 3251−3270.
(57) Pipe, C. J.; McKinley, G. H. Microfluidic rheometry. *Mechanics research communications* **2009**, *36*, 110−120.
(58) Zilz, J.; Schäfer, C.; Wagner, C.; Poole, R. J.; Alves, M. A.; Lindner, A. Serpentine channels: micro-rheometers for fluid relaxation times. *Lab Chip* **2014**, *14*, 351−358.

https://doi.org/10.1021/acs.macromol.2c00249
Macromolecules 2022, 55, 6031−6039